Desalination 508 (2021) 115048

Contents lists available at ScienceDirect

Desalination

journal homepage: www.elsevier.com/locate/desal

Computational fluid dynamic study on adsorption-based desalination and cooling systems with stepwise porosity distribution

Mingliang Li, Yanan Zhao, Rui Long *, Zhichun Liu, Wei Liu

School of Energy and Power Engineering, Huazhong University of Science and Technology, Wuhan 430074, PR China

HIGHLIGHTS

- Heat and mass transfer mechanism inside a finned-tube bed is revealed employing a CFD model.
- The influence of different stepwise distributions of bed porosity on AD system performances is systematically explored.
- The SCP and SDWP under the porosity distribution of D3-F are improved by 16.2%.
- A cooling effect of 0.219kW/kg and water throughput of 7.5m^3/ton-day are achieved.

ARTICLE INFO

Keywords:
Adsorption desalination
CFD model
Stepwise porosity
Finned-tube heat exchanger
Process optimization

ABSTRACT

Adsorption desalination (AD) is a promising alternative desalination technology with low energy cost. Conventional studies about AD cycle are mainly based on lumped models that do not involve the details of heat and mass transfer characteristics. In this study, a comprehensive analysis about the effect of stepwise porosity distributions inside a finned-tube bed on system performance is conducted with a transient computational fluid dynamic (CFD) model which captures the bed spatial temperature and pressure distributions, thus to reveal the heat and mass transfer mechanisms. Various bed porosity distribution scenarios at different packed directions are considered. Results reveal that all the forward distributions show an advanced cooling as well as water production. D3-F distribution results in the maximum specific cooling power (SCP) and specific daily water production (SDWP), presenting a 16.2% improvement over that of the uniform at the fin pitch of 55 mm. Moreover, system performances under various operating conditions including ad/desorption time, switch time and heating source temperature are evaluated. The system performance under optimal bed porosity distribution is tested with several adsorbents, among which silica gel of RD type shows a maximum cooling effect of 0.219 kW/kg and water throughput of 7.5 m^3/ton-day.

1. Introduction

Fresh water is the necessity of human life continuation. With expedited increase of water demand for agriculture, industrial and domestic applications, water obtaining is highly stressed [1–3]. However, only 2.5% of global natural water is potable water, most of the remaining (96.5%) is seawater. Desalination of saline or brackish water is getting more and more concern especially in the countries around desert or semi-arid areas. In the Gulf regions, as water scarcity under tropical desert climate, the shortfall of water supply can be solved by energy-intensive distillation of sea water [4].

Presently, many commercially available desalination methods are employed to meet the demand of fresh water. The reverse osmosis (RO) [5], which consumes mechanical energy to exert the hydrostatic pressure on a semipermeable membrane where only the smaller water molecules are permitted to pass through the pore to overcome the osmosis pressure, is the most utilized. The RO system has a proportion of around 59% in the total desalinated water production and more than 14,000 plants all over the world. Despite of wide utilization, the RO technology still has a lot of drawbacks such as high equipment maintenance, short membrane lifespan and the low water quality due to residual boron, chlorides and bromides. The multi-stage flash (MSF) is an extensively used thermal-driven desalination method, which shares 27% of the desalinated water production [6]. It can be amalgamated with a thermal plant and utilize the waste heat from fossil fuel combustion to

* Corresponding author.
E-mail address: r_long@hust.edu.cn (R. Long).

https://doi.org/10.1016/j.desal.2021.115048
Received 5 December 2020; Received in revised form 7 February 2021; Accepted 2 March 2021
0011-9164/© 2021 Elsevier B.V. All rights reserved.

Nomenclature

C_p	Specific heat, J kg^{-1} K^{-1}
COP	Coefficient of performance, –
d_p	Particle diameter, m
D_s	Mass diffusivity, m^2 s^{-1}
D_{so}	Pre-exponential factor, m^2 s^{-1}
E	Characteristic energy, J mol^{-1}
E_a	Activation energy, J mol^{-1}
H_a	Heat of adsorption, J kg^{-1}
h_{fg}	Latent heat of vaporization, J kg^{-1}
h	Convective heat transfer coefficient, W m^{-2} K^{-1}
K	Permeability, m^2
k	Thermal conductivity, W m^{-1} K^{-1}
M, m	Mass, kg
Nu	Nusselt number, –
n	Surface heterogeneity factor of the adsorption materials, –
P	Pressure of adsorption/desorption, Pa
P_s	Saturation pressure, Pa
Q	Heat, J
Q_{st}	Isosteric heat of adsorption, kJ kg^{-1}
R	Universal gas constant, J mol^{-1} K^{-1}
SCP	Specific cooling power, kW/ kg
SDWP	Specific daily water production, m^{-3} ton^{-1} day^{-1}
T	Temperature, K
t	Time, s
U	Velocity vector, m s^{-1}
X	Water uptake, kg kg^{-1}
X_∞	Maximum adsorbent capacity, kg kg^{-1}
X_o	Equilibrium uptake, kg kg^{-1}

Greek Symbols

ε	Porosity, –
μ	Dynamic viscosity, Pa s
ρ	Density, kg m^{-3}
α	Thermal diffusivity, m^2 s^{-1}

Subscripts

ads	Adsorption
b	Bed
c	Cooling
con	Condenser
des	Desorption
eva	Evaporation
e	Evaporator
f	Fluid
g	Gas phase
i	Initial
m	Metal
p	Particle
sat	saturation
s	Solid phase, saturated, saline
t	Total
v	Vapor phase
w	Water

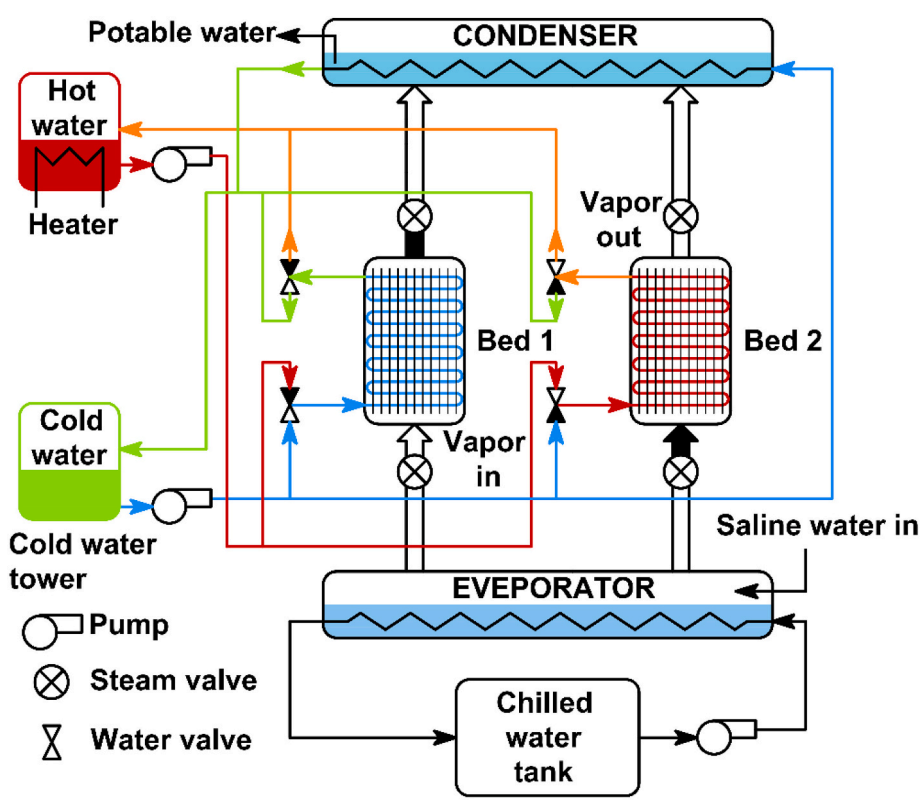

Fig. 1. Schematic of adsorption-based cooling and desalination system.

produce water and power simultaneously. However, it still consumes a lot of energy to produce desalinated water. Other desalination technologies including multi-effect distillation (MED) [7], electro-dialysis (ED) [8] have the same problem. Therefore, many researchers try to find a potentially alternative desalination technology with comparatively low energy cost and high water quality, the adsorption desalination (AD) has gained particular interest [9–11].

As shown in Fig. 1, the AD system consists of three main components: adsorber, evaporator and condenser [12–15]. Saline water is charged into the evaporator and vaporizes under the driving force of hydrophilic adsorbent particles. Cold water flows around the adsorbent bed to remove the adsorption heat, meanwhile the water evaporation generates cooling as a byproduct. After that the valve to the evaporator closes and hot water replaces the coolant to preheat the bed. Then adsorption chamber will be connected to the condenser where the desorbed vapor condenses to generate potable water, which has been experimentally demonstrated to be deionized water quality. Finally, circulation of cold water chills the bed to prepare for the next cycle. In this cooling and desalination cycle, heat energy is consumed to promote the desorption process and potable water production. As low-grade heat like waste heat or solar energy is consumed [16,17], the AD system costs only 1.38 kWh of electrical energy to pump the water cycle and 38.8 kWh of thermal power to produce one cube meter potable water, which is far less than that consumed by MSF (43.21 kWh of thermal energy) and MED (57.14 kWh of thermal energy) [18]. Compared with traditional vapor compression cooling cycle, water vapor achieves a pressure lift via the adsorption and desorption process, which gives the AD system many other advantages, such as low operating costs, few moving parts, simple control and vibration-free operation [19]. Adsorption desalination is an emerging low cost and environment friendly cooling and desalination technology with cycle activation from low grade heat, which has advantages in attenuating global warming [20]. This system produces high-grade potable water via the desorption-condensation process and cooling effect as a byproduct via the adsorption-evaporation process [21], which is fairly appropriate for some desert and coastal regions. Nevertheless, due to the heat and mass transfer resistance inside the porous media, the AD system has a low water throughput, which is the fundamental obstacle of its commercialization.

Many literatures highlighting the effect of adsorbent types on the performance of AD system have been reported [22]. Youssef et al. [18] compared the performance between AD system using silica gel and AQSOA-Z02 which is characterized by a monolayer-multi-layer adsorption mechanism at low pressure and a micropore filling at comparatively higher pressure. The results showed that AQSOA-Z02 performs better in terms of cooling effect and water production at a chilled water below 20 °C, compared with silica gel. Aluminum fumarate, a highly hydrophilic adsorbent, has obtained particular interest in recent adsorption studies [23–25]. Elsayed et al. [26] experimentally tested an AD system using aluminum fumarate adsorbent and compared it with conventional silica gel systems, the exceptional performance demonstrated its superiority. Other metal-organic frameworks (MOF) [27] like CPO-27, MIL-101, UIO-66 used in AD application were also investigated [28,29]. Among the adsorbents, Silica gel was fairly well developed in adsorption systems with low regeneration temperature and reasonable working capacities [30]. Studies about optimization of working conditions on a silica-gel-based adsorption system have been extensively carried out to improve its performance. Miyazaki et al. [31] proposed a new cycle time allocation considering the reduction of chilled water fluctuations. The new system had a 6% improvement in the cooling capacity. Thu et al. [32] established a heat recovery circuit between the evaporator and condenser to drive the AD dedicatedly produce water. The advanced system was capable of producing 9.24 m^3 potable water per ton silica gel per day, which was almost twice that of prior systems. Subsequently, they proposed a new heat recovery scenario using an encapsulated evaporator-condenser unit to further elevate the evaporator temperature [33]. The new integrated, straightforward heat recovery system resulted in a fairly high water throughput of 14.2 m^3/ton-day.

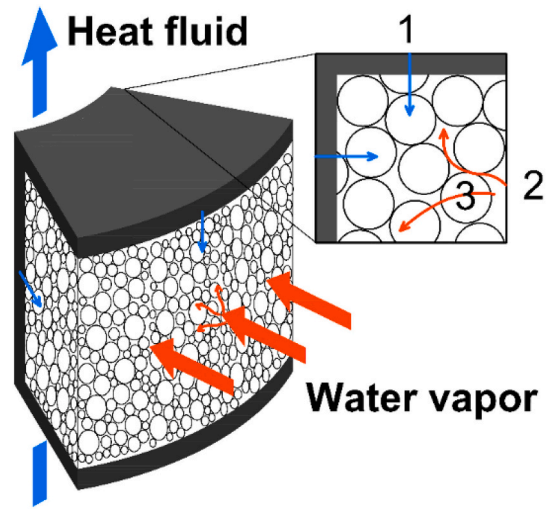

Fig. 2. Heat and mass transfer mechanisms in a finned-tube bed. 1: heat transfer between aluminum and silica gel particles; 2: inter-particle permeation; 3: intra-particle diffusion.

A single-stage AD system with more than two beds can produce cooling and water in a continuous manner, while a single-stage adsorption-based cooling and desalination system with air-cooled heat exchanger cannot work under tropical conditions according to the research of Mitra et al. [34], multi-stage system is more stabilized due to its lower pressure difference in each stage. Chakraborty et al. [35] proposed a double-stage AD system using AQSOA-Z02 and silica gel in different stage. With heat recovery circulation between condenser of stage 1, evaporator and condenser of stage 2, the system produced cooling effect and a bit of desalinated water in stage 1 whilst stage 2 produced water dedicatedly. Moreover, the results showed that using AQSOA-Z02 in stage 1 and silica gel in stage 2 can obtain the largest cooling and water production. Youssef et al. [36] developed a four-bed, two-stage AD system with an integrated evaporator-condenser unit as the intermediate level. The new cycle produced large amounts of cooling effect and desalinated water simultaneously.

It should be emphasized that the aforementioned studies are mainly based on a lumped model where the spatial temperature and pressure distributions inside the bed are not considered. Wu et al. [37] established a computational fluid dynamic (CFD) model to describe the heat and mass transfer mechanisms of a cylindrical annulus adsorbent bed. The effect of cycle time on the system performances is discussed in the literature. Other bed configurations especially the spatial porosity distributions are not considered, which can highly impact the heat and mass transfer process, thus the cooling and water production of the AD system. In present study, a CFD model considering the inter and intra-grain mass transfer resistances (as shown in Fig. 2) and time-depended evaporation pressure is established on a finned-tube heat exchanger filled with adsorbent particles [38] to explore effects of spatial porosity distributions on the performances of AD cycle and the advanced cooling and water production reveal it as an alternative manner to promote the throughput of AD system. A parametric analysis is conducted to determine the optimized working conditions, and some useful conclusions are drawn.

2. System description and modeling

2.1. Description of combined desalination and cooling system

The adsorption or desorption is conducted within a finned-tube heat

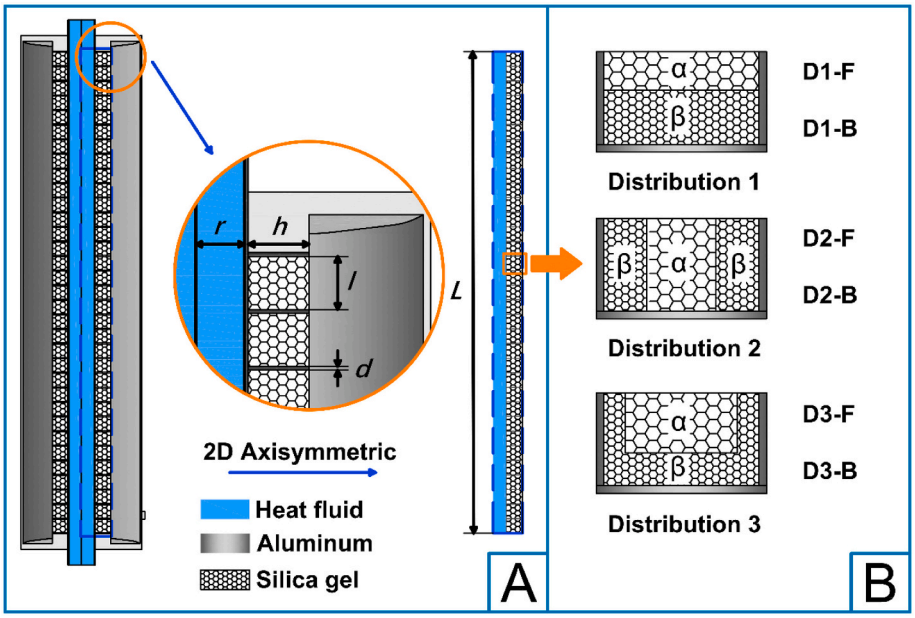

Fig. 3. Schematic of the simulated finned-tube bed (A) and the proposed several porosity distributions (B).

exchanger in which spherical silica-gel grains are filled in the gaps between fins. The bed geometric parameters are presented in Table 2. As shown in Fig. 3A, cooling/heating fluid alternatively flows inside the tube, assisting the hydrophilic adsorbent to capture/release vapor. In order to reduce the computational cost, the finned-tube bed is simplified to a two-dimensional axisymmetric model, as presented in Fig. 3A. As mentioned above, an adsorption-based cooling and desalination cycle consists of four steps, the adsorption-assisted water evaporation and simultaneous cooling, desorption-condensation accompanied with potable water production, and precooling/preheating between adsorption and desorption.

Fig. 3B presents the proposed three bed porosity distributions which are selected in accordance with the heat transfer characteristics of the finned-tube bed. Compared with the uniform condition, the porosity of α or β is fixed at 0.55 or 0.25 with average bed porosity kept constant. All the distributions consist of a forward and backward configuration, the former has a lower porosity adjacent to the metal surface, which promotes the heat transfer process.

Instead of lumped model used in previous studies, the adsorbent bed investigated in this paper has spatial temperature and pressure distributions. Consequently, the physical parameters vary spatially, which requires a lot of computation resource. In order to simplify the calculation, the following assumptions and simplifications are considered in the modeling [39].

1. The adsorbent particles are ideal spheres with constant diameter.
2. The pressure drop in the vapor pipe is neglected.
3. The gaseous of the adsorbent is assumed as an ideal gas phase.
4. Thermal conductivity, specific heat capacity and viscosity are independent of temperature.
5. The thermal resistance at all phase interfaces is neglected.
6. The water temperature is invariable in the cooling/heating process.
7. The convective heat transfer coefficient is constant inside the tube, the impact of fouling on the evaluation of overall heat transfer coefficient is neglected.

2.2. Governing equations

The adsorption process basically consists of two steps, an inter-particle permeation and an intra-particle diffusion. As the vapor velocity through the porous bed is relatively slow, the effect of inertial force can be neglected. The inter-particle mass transfer resistance is described using Darcy's law to obtain the vapor velocity through the bed.

$$\vec{U} = -\frac{K}{\mu}\nabla P \tag{1}$$

where μ is the water vapor viscosity, K the permeability of the bed, which can be calculated using the Blake-Kozeny equation.

$$K = \frac{d_p^2 \varepsilon_b^3}{150(1-\varepsilon_b)^2} \tag{2}$$

where d_p is the adsorbent particle diameter, ε_b the bed porosity.

The intra-particle mass diffusion is captured via a linear driving force (LDF) model, which is widely used in simulating the adsorption reaction kinetics with relatively low computational cost and high accuracy.

$$\frac{\partial X}{\partial t} = \frac{60 D_s}{d_p^2}(X_o - X) \tag{3}$$

where X is the water vapor uptake, X_o the uptake at adsorption equilibrium, D_s the surface diffusivity which can be estimated by:

$$D_s = D_{so} exp\left(-\frac{E_a}{RT_s}\right) \tag{4}$$

where D_{so} is the pre-exponential factor, E_a the activation energy of the

Table 1
The thermophysical parameters of silica gel.

$C_{ps}\left(\frac{kJ}{kg\cdot K}\right)$	$E_a\left(\frac{J}{mol\cdot K}\right)$	$D_{so}\left(\frac{m^2}{s}\right)$	$\rho_b\left(\frac{kg}{m^3}\right)$	$d_p(mm)$	$k_b\left(\frac{W}{m}\cdot K\right)$	$H_a\left(\frac{kJ}{kg}\right)$	$X_\infty\left(\frac{kg_v}{kg_a}\right)$	$E\left(\frac{J}{mol}\right)$	n
924	42,000	2.54×10^{-4}	740	0.35	0.198	2415	0.37	4280	1.15

Table 2
The bed geometric and model parameters.

L (mm)	r (mm)	h (mm)	l (mm)	d (mm)	T_{eva} (°C)	T_{con} (°C)	T_{hw} (°C)	T_{cw} (°C)	h (W/m^2·K)
560	13	12	15–55	1	15	25	65–95	25	500

Table 3
Initial and boundary conditions

Initial conditions	
$P = P_{sat}@T_{eva}$; $X = X_0@(T = 60\ °C, P = P_{eva})$; $T = T_{cw}$; $M_{sw} = M_0$	
Boundary conditions	
In the isobaric heating process	$T_f = T_{hw}$
In the desorption process	$T_f = T_{hw}$; $P(R) = P_{con}$
In the isobaric cooling process	$T_f = T_{cw}$
In the absorption process	$T_f = T_{hw}$; $P(R) = P_{eva}$

reaction, T_s the adsorbent temperature.

The equilibrium uptake can be captured using an equilibrium adsorption relation, the D-A equation [40].

$$X_o = X_\infty exp\left(-\left(\frac{RT_s}{E}ln\left(\frac{P_s}{P}\right)\right)^n\right) \tag{5}$$

where X_∞ is the maximum uptake of silica gel, E the characteristic energy, R the universal gas constant, n the heterogeneity factor, P the vapor pressure, and P_s the saturated pressure of water vapor of the bed temperature. Thermophysical parameters used in the modeling are listed in Table 1.

Apart from the reaction kinetic and thermodynamic equations, the adsorption process, a period involved both heat and mass transfer, should fit mass and energy conservation equations. Moreover, the heat conductions of aluminum tube and fin should also be considered.

The fluid mass conservation equation of the adsorbate gas is [41,42]:

$$\frac{\partial(\varepsilon_t\rho_v)}{\partial t} + \nabla\cdot\left(\rho_v\vec{U}\right) + \rho_b\frac{\partial X}{\partial t} = 0 \tag{6}$$

where ρ_v is the vapor density, ρ_b the bed density, $\vec{U}$ is the vapor velocity vector which can be obtained from the Darcy's law, ε_t is the total porosity which can be calculated by the particle porosity ε_p and bed porosity ε_b: $\varepsilon_t = \varepsilon_b + \varepsilon_p(1 - \varepsilon_b)$.

The energy conservation equation of the adsorbent bed is [43]:

$$\left(\varepsilon_b\rho_v C_{pv} + \rho_b C_{ps} + \rho_b X C_{pw}\right)\frac{\partial T_v}{\partial t} + \rho_v C_{pv}\vec{U}\cdot\nabla T = \nabla\cdot\left(k_{eff}\nabla T\right) + \rho_b H_a\frac{\partial X}{\partial t} \tag{7}$$

where C_{ps} is the specific heat capacity of adsorbent solid, H_a the isosteric adsorption heat.

The heat conduction differential equation of the aluminum tube and fin is [44,45]:

$$\frac{\partial T}{\partial t} = \alpha\nabla^2 T \tag{8}$$

where α is the thermal diffusivity of aluminum material.

2.3. Boundary conditions

During the adsorption process, the outside coolant flows into the tube at a temperature of 25 °C. The convective heat transfer coefficient is 500 W/m^2·K [46]. The sea water is concentrated as the water evaporates. Here the evaporation temperature is set at 15 °C. The evaporation pressure (P_{eva}) varies timely, which can be captured via the relationship between the partial vapor pressure and concentrations [47].

$$P_{eva} = (1 - 0.537S)P_{sat} \tag{9}$$

where $P_{sat} = 8.143 \times 10^{10}\ \exp(-5071.7/T)$ is the saturation pressure at temperature T. And S is the salinity.

During the desorption process, hot water with temperature varying from 65 °C to 95 °C flows in to the tube at a convective heat transfer coefficient set at 500 W/m^2·K. The pressure at outside of the bed is calculated by the condenser temperature of 25 °C. During switching processes, the outside of the bed is considered as isolated. The bed is still cooled by the external coolant or heated by the external hot water. All these parameters are presented in Table 2. The initial and boundary conditions are listed in Table 3.

2.4. Performance indicators

The system performance is examined in terms of specific cooling power (SCP), specific daily water production (SDWP) and coefficient of performance (COP). During the adsorption-evaporation or desorption-condensation process, the bed working capacity is equal to the amount of evaporated or condensed water, which directly generates cooling or the potable water. Consequently, all the performance parameters involved in this study are captured using the bed working capacity, as listed in the following three formulas.

$$SCP = \frac{h_{fg} \times \Delta X_{ad}}{t_{cycle}} \tag{10}$$

where ΔX_{ad} is the adsorption working capacity, t_{cycle} the cycle time, h_{fg} the latent heat of vaporization under the evaporator pressure.

$$SDWP = \frac{\Delta X_{des}}{\rho_w \times t_{cycle}} \tag{11}$$

where ΔX_{des} is the working capacity during desorption process, ρ_w the water density under the condenser temperature.

$$COP = \frac{Q_0}{Q_h} = \frac{\Delta X_{ad} \times h_{fg}}{\int_0^{t_{cycle}} q_h dt} \tag{12}$$

where q_h is the boundary heat flux of the heating process.

3. Results and discussion

Several stepwise porosity configurations are proposed in accordance

Table 4
Default designing and operation parameters.

Optimized parameter	Fin pitch (mm)	Ad/desorption time (s)	Switch time (s)	Heat source temperature (°C)	Adsorbent
Fin pitch (mm)	13–55	500	20	85	Silica gel
Ad/desorption time (s)	27	100–1100	20	85	Silica gel
Switch time (s)	27	500	10–50	85	Silica gel
Heating source temperature (°C)	27	500	20	65–95	Silica gel

Table 5
Effect of mesh points and time step on simulation results.

Time step	0.5 s						1.0 s					
Mesh size	5500		10,560		20,540		5500		10,560		20,540	
Time	X_{av}	T_{av}	X_{av}	T_{av}	X_{av}	T_{av}	X_{av}	T_{av}	X_{av}	T_{av}	X_{av}	T_{av}
100	0.1032	321.72	0.1032	321.73	0.1033	321.74	0.1032	321.72	0.1032	321.73	0.1033	321.74
300	0.1274	317.55	0.1273	317.56	0.1273	317.57	0.1274	317.55	0.1273	317.56	0.1273	317.57
500	0.1448	314.71	0.1448	314.72	0.1447	314.73	0.1448	314.71	0.1448	314.72	0.1448	314.73

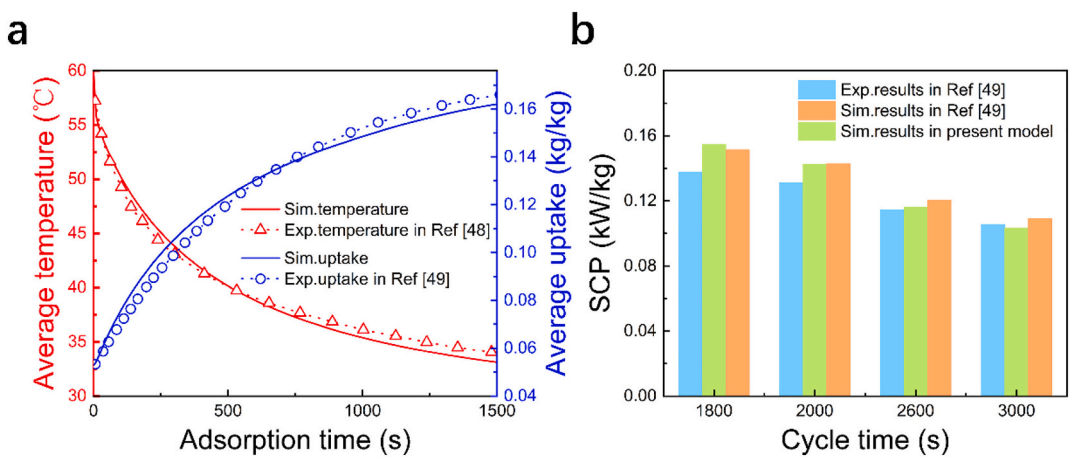

Fig. 4. Comparison between the simulation and experimental results.

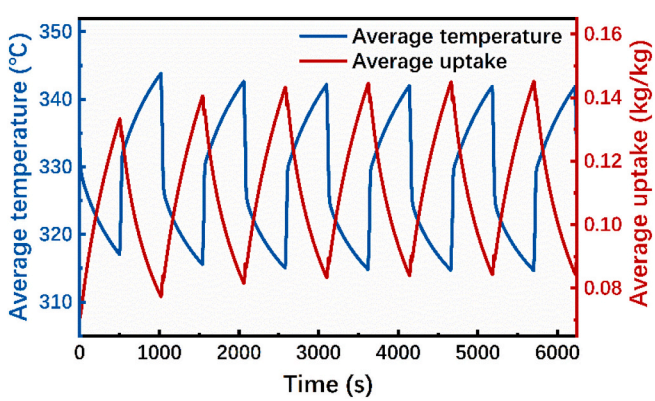

Fig. 5. Temporal histories of bed average temperature and uptake from transient to cyclic steady state.

with the characteristics of tube-fin heat exchangers. We start with the effect of fin pitch on system performances including SCP, SDWP and COP to obtain some differences between the stepwise distributions and the uniform distribution in the comparatively complicated transient heat and mass transfer process of the porous media. Subsequently, a parametric analysis in terms of ad/desorption time, switch time and heating source temperature is conducted to gain the optimized operating conditions. Finally, the performances of system using several adsorbents are compared to find an exceptional adsorbent at the optimal operating condition. All the default designing and operation parameters are listed in Table 4.

3.1. Mesh sensitivity and model validation

Table 5 presents the bed average temperatures and uptakes at different adsorption times of a steady cycle using several mesh size and time step configurations. The numerical results manifest that with a grid size of 10,560 and time step of 1.0 s, it is sufficient to obtain accuracy calculation results.

Fig. 4 depicts the comparison between the calculated data through present model and the experimental data in Refs. [48,49]. In Fig. 4a, the average temperature and uptake agrees well with those experimental data. In Fig. 4b, both the experimental and simulated data in previous literature are employed to validate the accuracy of the present model. The slight derivation between the calculated data in Ref. [49] and that in present originates from the difference in energy equations. The small deviation between the simulation and experiment results verifies the adsorption model employed in this study.

3.2. Dynamic characteristics

Fig. 5 shows the temperature-time and uptake-time histories of the adsorption bed within 6 cycles. The hot water temperature and fin pitch are set at 85 °C and 27 mm, respectively, whilst the ad/desorption time is fixed at 500 s and switch time 20 s. The system achieves a cyclic steady state after 5 to 6 adsorption cooling and desalination cycles at an initial bed temperature of 60 °C. During the adsorption process, the bed is cooled by the fluid flowing inside the tube, companied with the release of adsorption heat. Then the bed will go through preheating, desorption and precooling process after which the next cycle begins. Although bed temperature decreases in both adsorption and precooling process, with the release of latent heat (adsorption heat), the temperature drop during adsorption process is not as steeper as precooling process. There is a similar statement between the desorption and preheating process. In general, the precooling/heating process, a period of isolated and near-isosteric thermal swing, is companied with drastic temperature drop/lift whilst the bed total uptake varies a little. On the other hand, as the initial bed mass is kept at a constant value after the system stabilizes, adsorption capacity is equal to desorption capacity in this state, as seen in Fig. 5. Consequently, as all the system performance parameters are calculated at the cyclic steady state, both of SCP and SDWP can be obtained from adsorption capacity.

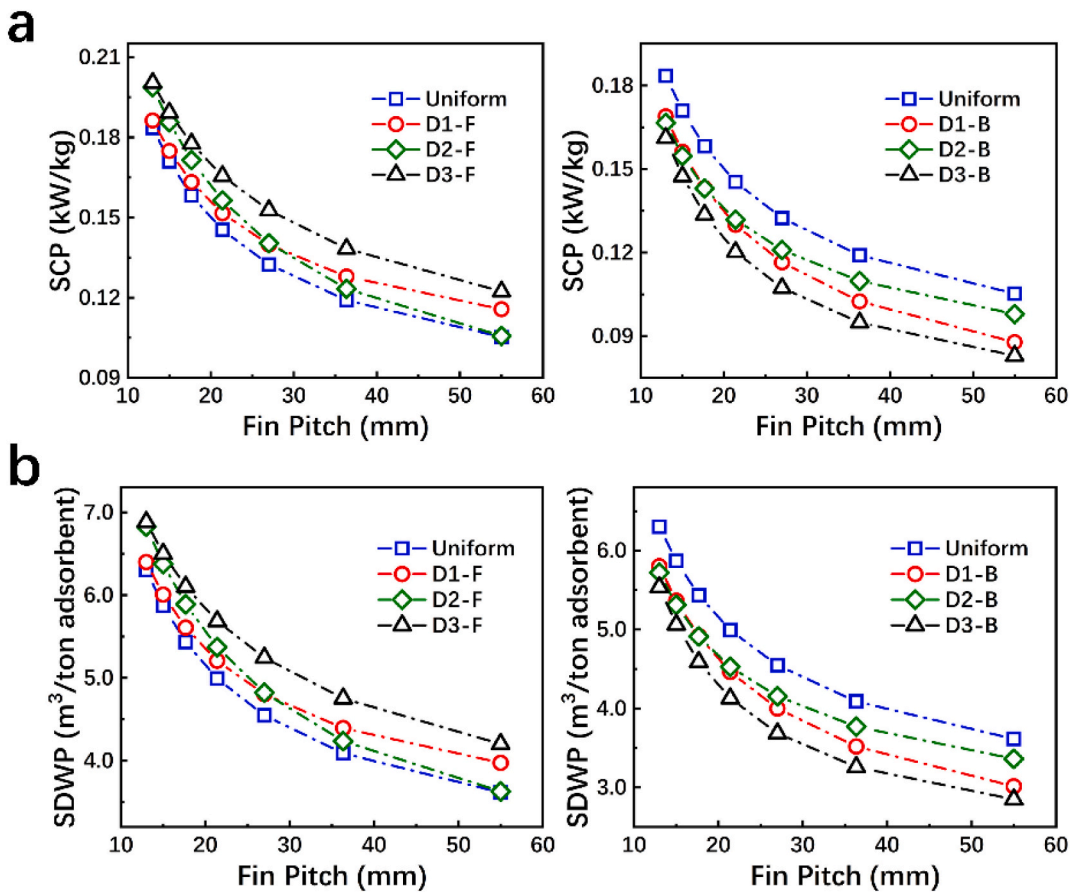

Fig. 6. Variations of (a) SCP; and (b) SDWP with the fin pitch for different bed porosity distributions.

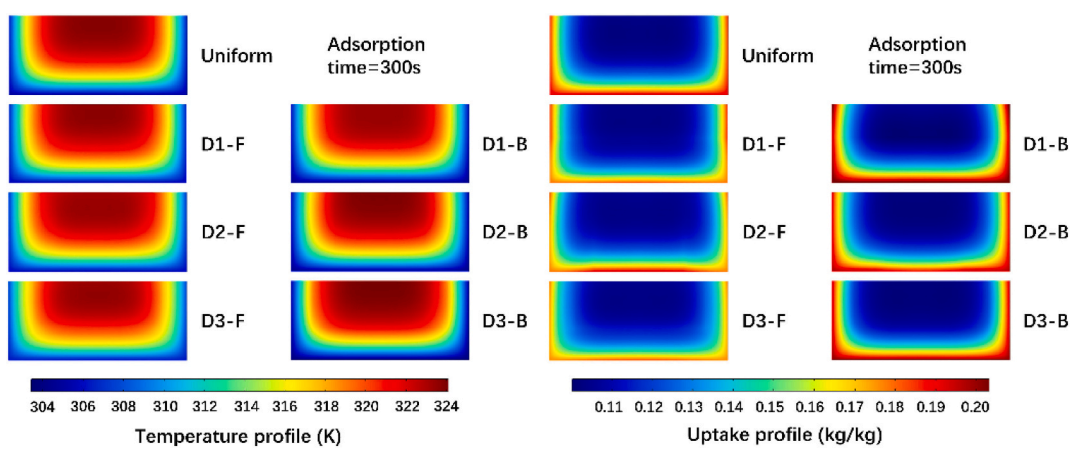

Fig. 7. Temperature profiles and uptake profiles for an adsorbent module under different bed porosity distributions at adsorption time of 300 s. In the simulation, the fin pitch is set at 27 mm.

3.3. The effect of fin pinch

Fig. 6(a) and (b) present SCP and SDWP variations in terms of fin pitch and bed porosity distribution. During the adsorption process, the kinetic energy of the water molecules is transformed to the adsorption heat, which rises the bed temperature. The reduction of fin pitch leads to augment the total heat transfer area, which will enhance the heat transfer coefficient between the adsorbent bed and the cooling fluid, thus the adsorption uptake. Based on Eqs. (10) and (11), both of SCP and SDWP vary with the adsorption uptake. Consequently, it can be observed from Fig. 6(a) and (b) that SCP and SDWP increase as the fin pitch decreases and their qualitative behavior is just the same.

As shown in Fig. 6(a) and (b), all the forward distributions (D1-F, D2-F, D3-F) make a higher SCP and SDWP than the uniform one. It should be noted that for all the distributions, the total bed porosity is kept at 0.4. Yet the forward distribution has a lower porosity near the heat exchange surface than the uniform or the backward (D1-B, D2-B, D3-B) distribution. In the simulation, the bed thermal conductivity can be calculated as the weighted average of the silica gel thermal conductivity and the vapor thermal conductivity.

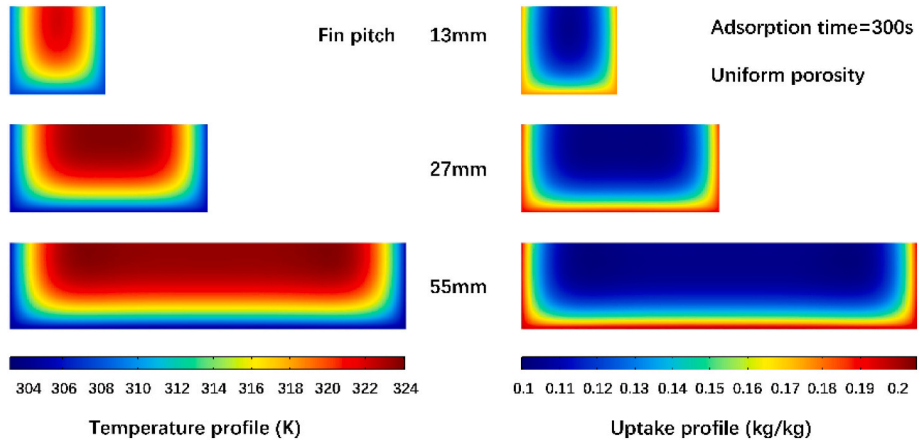

Fig. 8. Temperature profiles and uptake profiles for an adsorbent module under various fin pitches at adsorption time of 300 s. In the simulation, the bed has a uniform porosity.

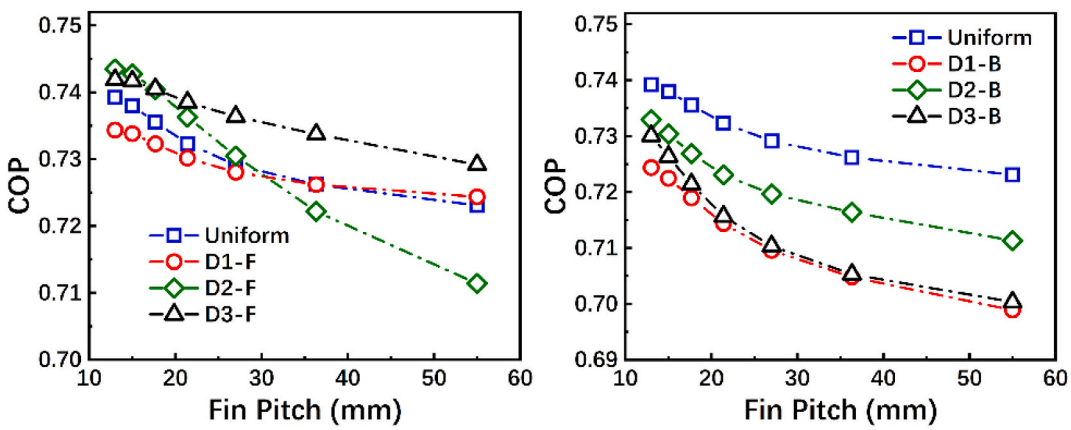

Fig. 9. Variations of COP with the fin pitch for different bed porosity distributions.

$$k_b = k_v \varepsilon_b + k_s(1 - \varepsilon_b) \tag{13}$$

where k_b is the bed thermal conductivity, k_s the silica gel thermal conductivity, k_v the vapor thermal conductivity, ε_b the bed porosity. Based on Eq. (13), the forward distribution has a higher thermal conductivity near the cooling/heating surface, which facilitates the discharge/supply of the adsorption/desorption heat. The temperature and uptake distributions for an adsorbent module with the same fin pitch of 27 mm are examined in Fig. 7 at the adsorption time of 300 s. The figure shows that the temperature in a bed with forward porosity distribution is comparatively more well-proportioned than a uniform or backward one, which then manifests the higher thermal conductivity of this configuration. Yet, their average temperature is almost the same, which arises due to the fact that enhancement of heat transfer occurs not only in the cooling but in the heating process, leading the forward distribution a higher initial bed temperature and cooling rate in the adsorption process, this also occurs in the uptake distribution as shown in Fig. 7. For different fin pitches, the temperature and uptake profiles are presented in Fig. 8. Evidently, a larger fin pitch leads to a reduction of heat transfer coefficient, which attenuates the rejection of adsorption heat and makes the bed a higher temperature, thus the lower adsorption uptake, as shown in Fig. 8.

Furthermore, it can be observed from Fig. 6(a) and (b) that the three porosity scenarios behave differently as the fin pitch changes. In general, among all the distributions, D3-F has the best performance and D3-B the worst. For the fin pitch of 55 mm, D3-F results in a SCP of 0.122 kW/kg and SDWP of 4.2 m^3 per ton silica gel per day, which is 16.2% higher than that of the uniform porosity, whilst D3-B is capable only of producing 0.083 kW/kg of cooling and 2.8 m^3 per ton silica gel per day of fresh water, which is 21.2% lower than that of the uniform condition. As for other two schemes, D2-F keeps a higher SCP and SDWP with the fin pitch variations up to around 28 mm, after that D2-F performs worse than D1-F. For example, for fin pitch of 13 mm, D2-F results in a SCP of 0.199 kW/kg and SDWP of 6.8 m^3 per ton adsorbent per day, whilst D1-F

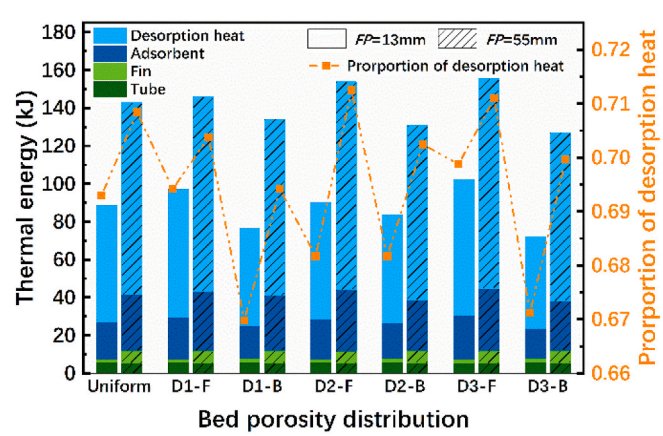

Fig. 10. Distribution of the supplied thermal energy and proportion of desorption heat for different bed porosity distributions at fin pitch of 13 mm and 55 mm.

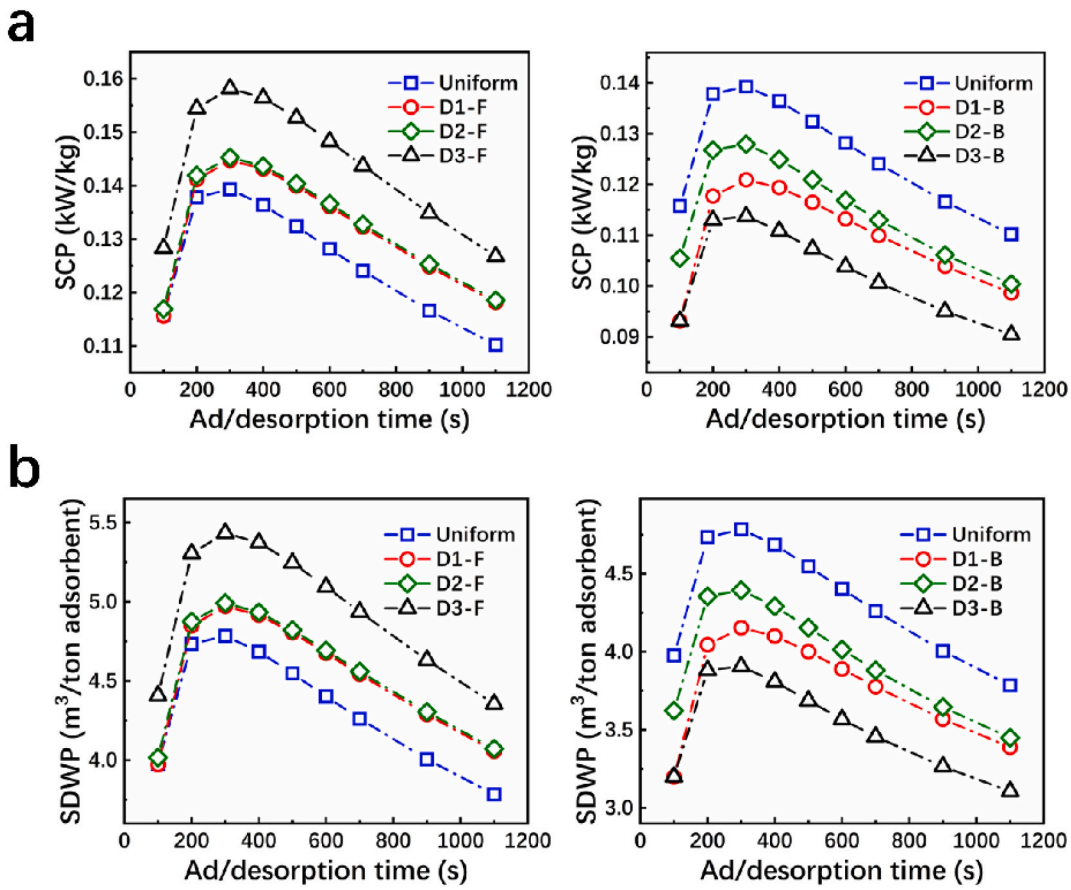

Fig. 11. Variations of (a) SCP; and (b) SDWP with the ad/desorption time for different bed porosity distributions.

produces 0.186 kW/kg of cooling and 6.4 m^3 per ton adsorbent per day of fresh water. Yet, D2-F results in a lower SCP and SDWP than D1-F for the fin pitch of 55 mm, where the former produces 0.106 kW/kg of cooling, 3.6 m^3 per ton adsorbent per day of water and the later results in a SCP of 0.116 kW/kg, SDWP of 4.0 m^3 per ton adsorbent per day. For D2-B and D1-B, there is a similar statement. In general, at shorter fin pitches, D2-F is more appropriate. As the adsorption or desorption is accompanied by generation or rejection of the isosteric adsorption heat, attenuating the heat transfer resistance causes an elevation of heat flux through the cooling/heating fluid, which will promote the ad/desorption process. Evidently, D3-F has optimized thermal conductivity near all the heat exchange surface, which results in a well-proportioned temperature and lower heat transfer resistance, thus the larger working capacity. For D2-F or D1-F, the thermal conductivity is optimized near the fin or tube. Consequently, since the fin pitch diminishes, the role of the heat exchange through the fin became more dominant, which makes D2-F better performance in terms of SCP and SDWP. The corresponding backward distributions of the three schemes are just the opposite.

The coefficient of performance is examined in Fig. 9. The figure shows that the increase in fin pitch leads to slight reduction in COP for almost all the porosity scenarios except D2-F, especially at larger fin pitches. For D2-F, COP almost diminishes linearly due to the increase in fin pitch. Based on Eq. (12), COP is the ratio of cooling capacity and the total supplied heat in a whole cycle. In the heating process, the total supplied heat is partly used for the bed different sections consisting of aluminum tube, fin and the silica gel adsorbent heat up and partly consumed for the desorption heat which is directly related to the cooling capacity at a cyclic steady state. Consequently, the distribution of the total supplied thermal energy consumed in the heating process is presented in Fig. 10 for better understanding of COP variation for each porosity distribution combined with fin pitch of 13 mm and 55 mm, respectively.

The figure shows that the proportion of the desorption heat decreases as the fin pitch augments, leading to a reduction of COP, as presented in Fig. 9. On the other hand, due to the lower proportion of desorption heat, all the backward distributions keep a lower COP. For the forward distributions, D3-F keeps a higher proportion of desorption heat and consequently COP than the uniform at all fin pitches. Yet, D1-F keeps a lower COP than the uniform condition with the fin pitch variations up to about 36 mm, after that D1-F performs slightly better than the uniform,

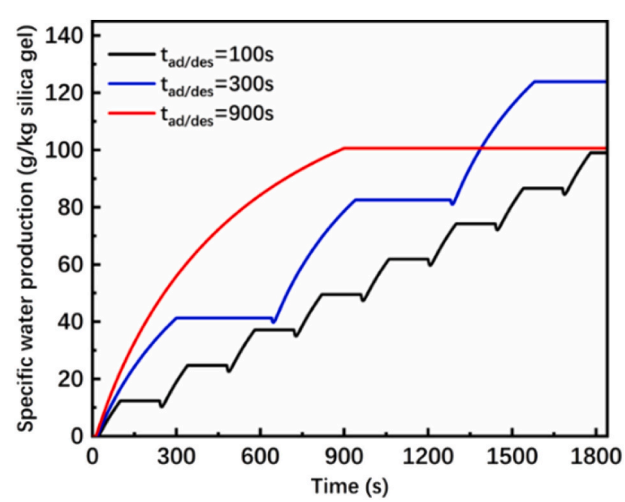

Fig. 12. Comparison of specific water production for the selected three adsorption/desorption times (100 s, 300 s, 900 s).

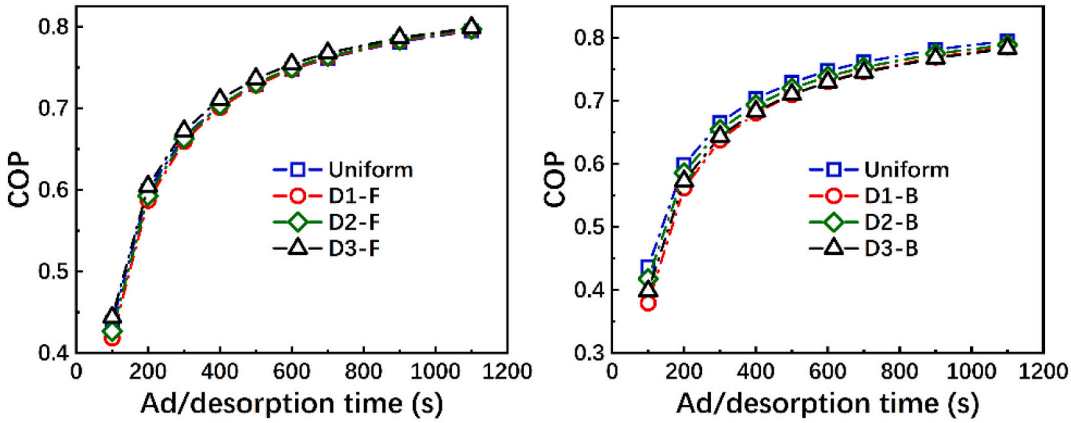

Fig. 13. Variations of COP with the adsorption/desorption time for different bed porosity distributions.

which is just the opposite in D2-F. These anomalies may arise due to the fact that inevitable gradient porosity distribution orthogonal to the other heat transfer direction will attenuate the heat transfer coefficient whilst the porosity distribution parallel one heat transfer direction is optimized in D1-F or D2-F. As heat transfer through the other direction becomes more predominant, the net effect is to attenuate the total heat transfer coefficient and consequently the proportion of desorption heat. This also accounts for the fact that COP is more sensitive with the variation of fin pitch in D2-F.

3.4. The effect of adsorption/desorption time

The SCP and SDWP variations with the adsorption/desorption time for different porosity distributions are depicted in Fig. 11. All the forward distributions result in a higher SCP and SDWP than the uniform or the backward one, as mentioned in Section 3.3. Yet this increase becomes less obvious at shorter ad/desorption time, especially for D1-F and D2-F, which is attributed to the predominant mass transfer resistance in this case as it is basically governed by the bed geometrical specifications and adsorbent grain size. On the other hand, it can be found from Fig. 11(a) and (b) that cooling capacity and water throughput do not vary with ad/desorption time in a monotonically manner. The best performance is observed for a cycle time of 300 s, where D3-F generates a maximum SCP of 0.158 kW/kg and SDWP of 5.4 m^3 per ton adsorbent per day.

A comparison of SWP (the specific water production) for three

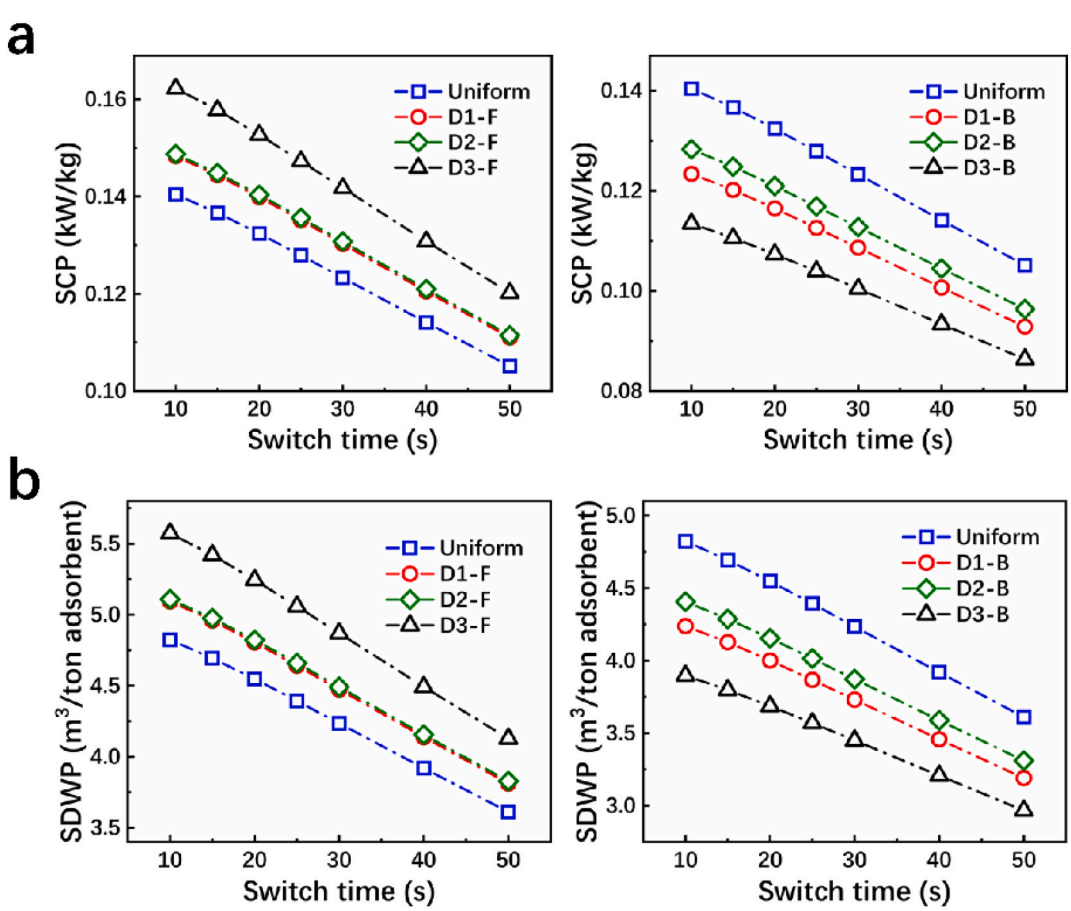

Fig. 14. Variations of (a) SCP; and (b) SDWP with the switch time for different bed porosity distributions.

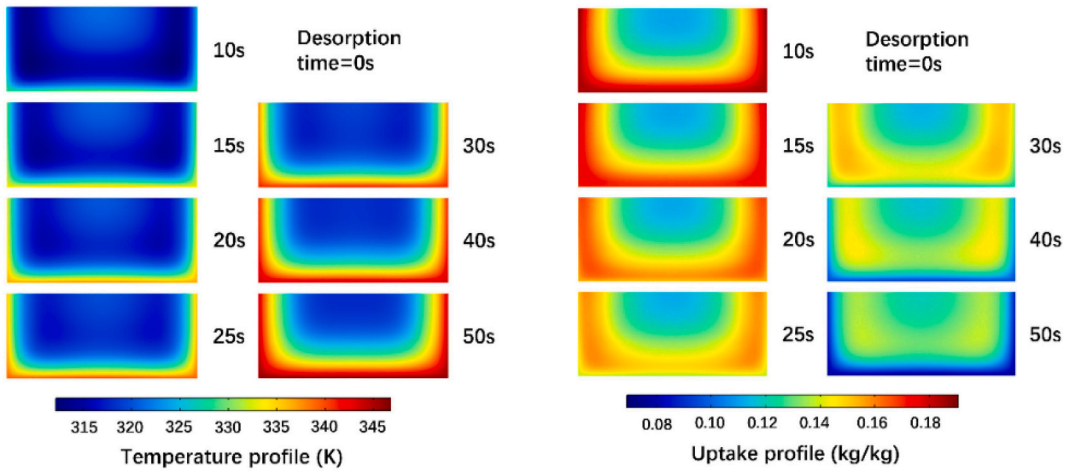

Fig. 15. Temperature profiles and uptake profiles for an adsorbent module at different switch time. In the simulation, the fin pitch is set at 27 mm.

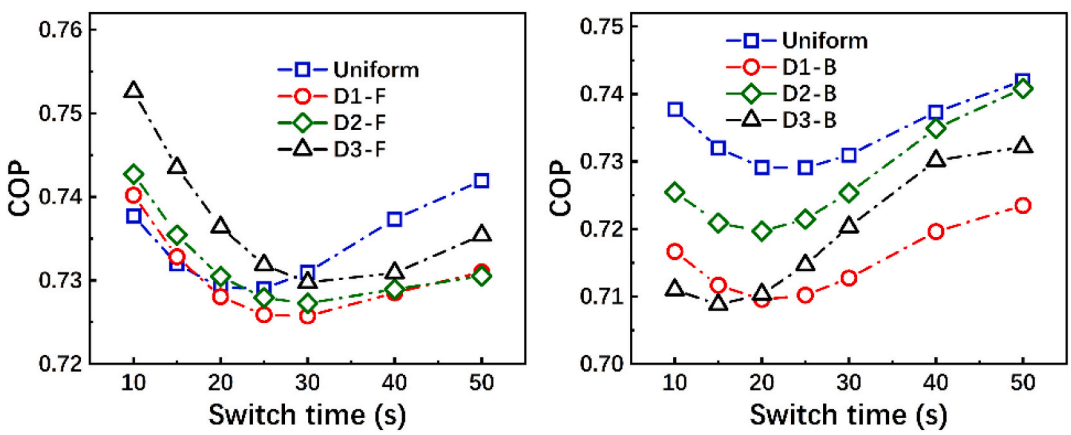

Fig. 16. Variations of COP with the switch time for different bed porosity distributions.

different ad/desorption times is presented in Fig. 12 for further understanding of this result. As mentioned in Section 2, the desalinated water is produced during the desorption process in which the released water vapor condensation and the silica gel adsorbent regeneration occur simultaneously. It can be found from Fig. 12 that longer ad/desorption time results in a higher SWP and silica gel recovery rate in one cooling cum desalination cycle. Nevertheless, long cycle time means a reduction of the number of cycles within a constant comparatively long time. The optimized cycle time balances the two fundamental elements, consequently, a maximum SCP and SDWP are produced by the system in which silica gel adsorbent is well dried and the number of cycles is appropriately configurated. Furthermore, it can be observed from Fig. 12 that a slight fluctuation occurs in the preliminary stage of desorption process. This discrepancy arises due to the insufficient pressure elevation during the preheating process in a single-stage system. Subsequently, when the outlet valve to the condenser opens, the bed pressure can't achieve the condenser pressure and water vapor starts to feed the adsorbent bed, which makes the vapor pressure instantaneously increase and the bed generally in a transient adsorption status.

Fig. 13 presents the coefficient of performance for different porosity configurations as a function of ad/desorption time. The figure shows that a longer ad/desorption time leads to the COP dramatic augment. For larger cycle time, the proportion of energy consumed for the metal and silica gel heat up in the total supplied heat decreases, at the same time the duration allowed for desorption is long enough to approach the uptake equilibrium. Both of them lead to higher proportion of desorption heat and COP. It should be noticed that the optimized ad/desorption time in terms of cooling capacity and water production results in a sub-optimal COP. Generally, simultaneous optimization of ad/desorption time both in SCP and COP is not practical. However, as depicted in Fig. 13, the COP is less sensitive to the ad/desorption time at a larger cycle time, which illustrates that it's not prudent to increase the cycle time further in order to obtain higher COP as the water production keeps attenuating.

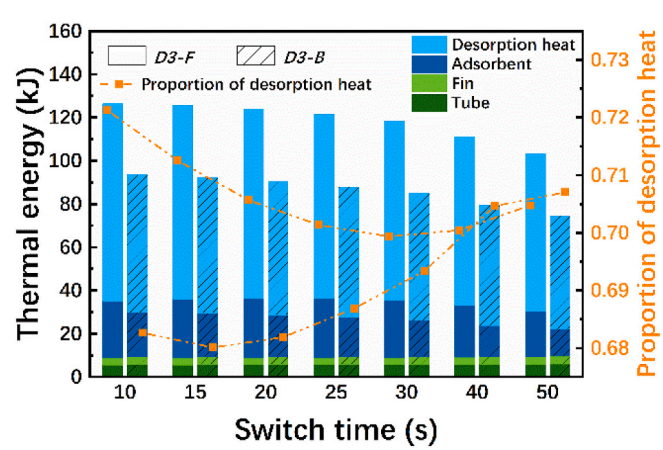

Fig. 17. Distributions of the supplied thermal energy and proportion of desorption heat for different switch times in D3-F and D3-B.

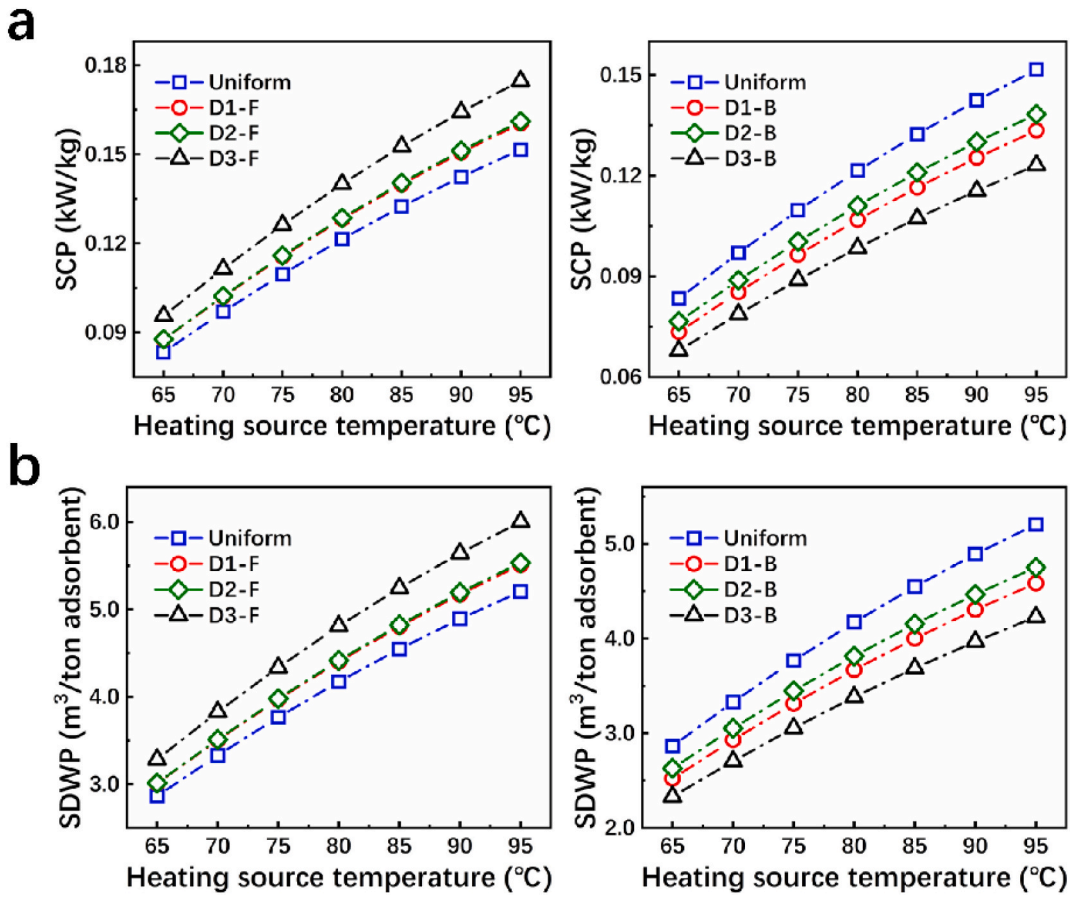

Fig. 18. Variations of (a) SCP; and (b) SDWP with the heating source temperature for different bed porosity distributions.

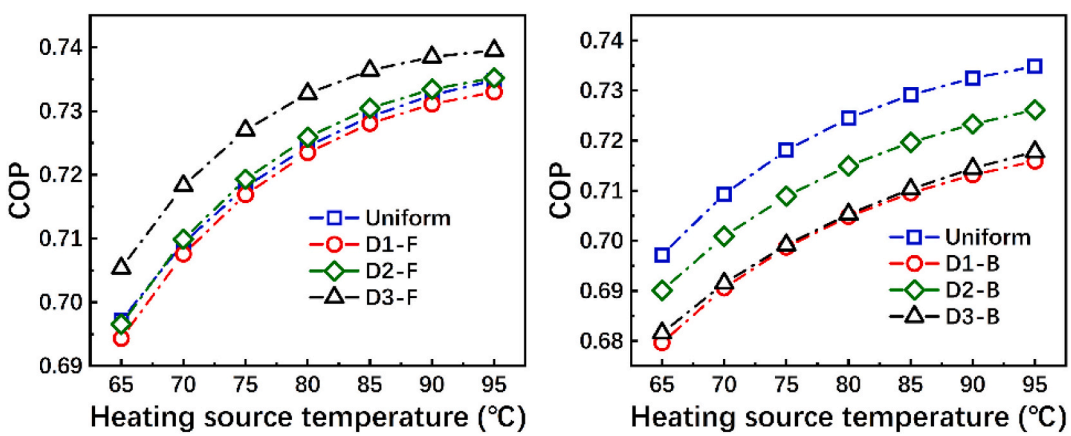

Fig. 19. Variations of COP with the heating source temperature for different bed porosity distributions.

3.5. The effect of switch time

As mentioned in Section 2, the adsorption bed will go through a precooling or preheating process before adsorption or desorption, after which the bed working status switches and the vapor valve to the evaporator or condenser opens. For adsorption chiller operation, a period of isolated, near-isosteric thermal swing is indispensable. During the preheating process, as a low thermal conductivity of the porous media, the temperature of adsorbent far from the aluminum surface is still at a comparatively lower value, which can be observed from the bed temperature profile in Fig. 15. As a result, the water vapor released from the adsorbent with a higher temperature (silica gel adjacent to the tube wall and fin) is partly adsorbed by this part, which has been demonstrated in [50]. Fig. 15 depicts the impact of different switch times on the temperature and uptake spatial distributions in an adsorbent module with the same fin pitch of 27 mm at the beginning of desorption process. It illustrates that longer switch time results in a higher initial temperature of desorption, thus leading to a reduction of uptake, especially in the vicinity of tube wall and fin. Consequently, the cooling capacity and desalinated water throughput almost diminish linearly due to the increase in switch time, as shown in Fig. 14(a) and (b). However, that does not mean the switch time can be diminished infinitely. As mentioned in Section 3.3, for a shorter switch time, the pressure lift in a single-stage system during the preheating process is insufficient, which may

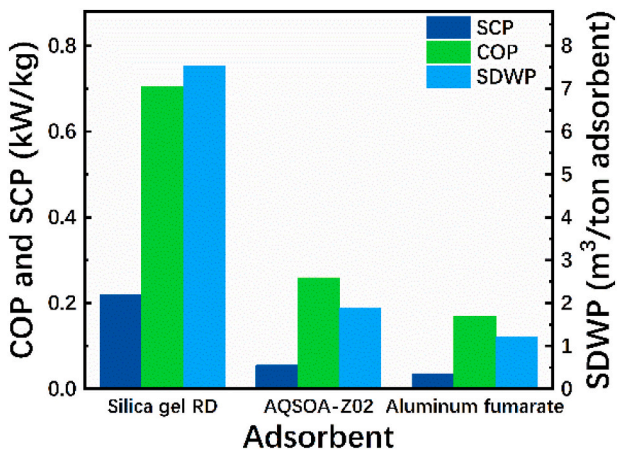

Fig. 20. Comparison of SCP, SDWP and COP for the selected three adsorbents.

eventually annul the desalinated water throughput of the system. For the system with a cycle time ranged from 600 s to 1200 s, the selected switch time in this paper is reasonable.

The variations of coefficient of performance with the switch time are examined in Fig. 16. It can be observed from the figure that COP and switch time are not linearly related. As mentioned prior, reduction of switch time leads the cooling capacity augment monotonically. However, as the ad/desorption time is kept constant, shorter switch time means insufficient heating or cooling in a whole steady cycle, which will cause a larger temperature difference between the heating water and the bed, thus inducing an elevation of total supplied heat in the non-equilibrium convection heat transfer, as presented in Fig. 17. Simultaneous increases of both cooling capacity and supplied energy make a minimum value exist in the curve. For further analysis, energy consumed by different components of D3-F and D3-B is depicted in Fig. 17. It elucidates that larger switch time and the backward configuration induce a reduction of supplied heat. On the other hand, the proportion of desorption heat, which directly reflects COP, shows a minimum value at a shorter switch time for D3-B. This may arise due to the fact that low wall-vicinity thermal conductivity of D3-B results in the attenuating of heat transfer coefficient, which is more significant at shorter switch time as it has a larger heat transfer temperature difference.

3.6. The effect of heat source

It has been illustrated in literatures that hot water temperature ranged from 65 °C to 95 °C is appropriate for a single-stage adsorption cooling cum desalination system using silica gel adsorbent. As shown in Fig. 18, cooling capacity and water throughput almost linearly augment with the hot water temperature. For example, D3-F results in a SCP of 0.111 kW/kg and SDWP of 3.8 m^3 per ton silica gel per day at 70 °C hot water temperature, whilst D3-F produces 0.153 kW/kg of cooling and 5.2 m^3 of potable water per ton silica gel per day at 85 °C hot water temperature. The effect of heating source temperature on the coefficient of performance of different porosity configurations is examined in Fig. 19. Both SCP and COP increase monotonically with the heating source temperature elevated, which is attributed to the promoted desorption process at higher hot water temperatures, leading to an increase in system performance. However, as the adsorption-based cooling and desalination system which is usually used in a low-grade heat condition, hot water temperatures below 85 °C are more appropriate.

3.7. Performance under different adsorbents

The performances of systems using silica gel of RD type, AQSOA-Z02 and Aluminum fumarate are compared in Fig. 20, at the optimal operating conditions investigated above. The result shows that silica gel produces a much larger cooling of 0.219 kW/kg and water throughput of 7.5 m^3/ton-day than that of AQSOA-Z02 and Aluminum fumarate. Evidently, the proposed optimal operating conditions are not appropriate for the other two adsorbents, as they have a smaller adsorption rate, and thus a longer cycle time, moreover, AQSOA-Z02 needs a lower chilled water temperature whilst a higher heating source temperature leads Aluminum fumarate an enhanced performance.

4. Conclusions

In this study, a comprehensive analysis about the effect of stepwise porosity distributions inside a finned-tube bed on system performance is conducted with a transient CFD model which captures the bed spatial temperature and pressure distributions, thus to reveal the heat and mass transfer mechanisms. Various bed porosity distribution scenarios at different packed directions are considered. Results reveal that all the forward distributions show an advanced cooling as well as water production. D3-F distribution results in the maximum SCP and SDWP, presenting a 16.2% improvement over that of the uniform at the fin pitch of 55 mm. As for other two schemes, D2-F keeps a higher SCP and SDWP with the fin pitch variations up to around 28 mm, after that D2-F performs worse than D1-F, which illustrates the superiority of D2-F at shorter fin pitches. Moreover, system performances under various operating conditions including ad/desorption time, switch time and heating source temperature are evaluated. The system performance under optimal bed porosity distribution is tested with several adsorbents, among which silica gel of RD type shows a maximum cooling effect of 0.219 kW/kg and water throughput of 7.5 m^3/ton-day.

CRediT authorship contribution statement

Mingliang Li: Writing - Original draft. **Yanan Zhao**: Visualization. **Rui Long**: Conceptualization, Writing - Review & Editing. **Zhichun Liu**: Investigation. **Wei Liu**: Formal analysis.

Declaration of competing interest

The authors declare no competing financial interest.

Acknowledgements

This work was financially supported by the National Natural Science Foundation of China (51736004).

References

[1] K.C. Ng, K. Thu, S.J. Oh, L. Ang, M.W. Shahzad, A.B. Ismail, Recent developments in thermally-driven seawater desalination: Energy efficiency improvement by hybridization of the MED and AD cycles, Desalination 356 (2015) 255–270.
[2] Z. Kuang, R. Long, Z. Liu, W. Liu, Analysis of temperature and concentration polarizations for performance improvement in direct contact membrane distillation, Int. J. Heat Mass Transf. 145 (2019), 118724.
[3] S. Lin, H. Zhao, L. Zhu, T. He, S. Chen, C. Gao, et al., Seawater desalination technology and engineering in China: a review, Desalination 498 (2021), 114728.
[4] B.B. Saha, I.I. El-Sharkawy, M.W. Shahzad, K. Thu, L. Ang, K.C. Ng, Fundamental and application aspects of adsorption cooling and desalination, Appl. Therm. Eng. 97 (2016) 68–76.
[5] D.R. Prathapaneni, K. Detroja, Optimal design of energy sources and reverse osmosis desalination plant with demand side management for cost-effective freshwater production, Desalination 496 (2020).
[6] A. Al-Othman, M. Tawalbeh, M. El Haj Assad, T. Alkayyali, A. Eisa, Novel multi-stage flash (MSF) desalination plant driven by parabolic trough collectors and a solar pond: a simulation study in UAE, Desalination 443 (2018) 237–244.
[7] K. Thu, Y.-D. Kim, G. Amy, W.G. Chun, K.C. Ng, A hybrid multi-effect distillation and adsorption cycle, Appl. Energy 104 (2013) 810–821.
[8] O.S. Burheim, F. Seland, J.G. Pharoah, S. Kjelstrup, Improved electrode systems for reverse electro-dialysis and electro-dialysis, Desalination 285 (2012) 147–152.
[9] K. Thu, A. Chakraborty, Y.-D. Kim, A. Myat, B.B. Saha, K.C. Ng, Numerical simulation and performance investigation of an advanced adsorption desalination cycle, Desalination 308 (2013) 209–218.

[10] J.W. Wu, M.J. Biggs, P. Pendleton, A. Badalyan, E.J. Hu, Experimental implementation and validation of thermodynamic cycles of adsorption-based desalination, Appl. Energy 98 (2012) 190–197.
[11] J.W. Wu, E.J. Hu, M.J. Biggs, Thermodynamic cycles of adsorption desalination system, Appl. Energy 90 (1) (2012) 316–322.
[12] A. Askalany, E.S. Ali, R.H. Mohammed, A novel cycle for adsorption desalination system with two stages-ejector for higher water production and efficiency, Desalination 496 (2020).
[13] R. Long, X. Xia, Y. Zhao, S. Li, Z. Liu, W. Liu, Screening metal-organic frameworks for adsorption-driven osmotic heat engines via grand canonical Monte Carlo simulations and machine learning, iScience 24 (1) (2021), 101914.
[14] Y. Zhao, Z. Luo, R. Long, Z. Liu, W. Liu, Performance evaluations of an adsorption-based power and cooling cogeneration system under different operative conditions and working fluids, Energy 204 (2020), 117993.
[15] Y. Zhao, M. Li, R. Long, Z. Liu, W. Liu, Dynamic modelling and analysis of an adsorption-based power and cooling cogeneration system, Energ. Convers. Manag. 222 (2020), 113229.
[16] A.S. Alsaman, A.A. Askalany, K. Harby, M.S. Ahmed, Performance evaluation of a solar-driven adsorption desalination-cooling system, Energy 128 (2017) 196–207.
[17] K. Thu, B.B. Saha, K.J. Chua, K.C. Ng, Performance investigation of a waste heat-driven 3-bed 2-evaporator adsorption cycle for cooling and desalination, Int. J. Heat Mass Transf. 101 (2016) 1111–1122.
[18] P.G. Youssef, S.M. Mahmoud, R.K. Al-Dadah, Performance analysis of four bed adsorption water desalination/refrigeration system, comparison of AQSOA-Z02 to silica-gel, Desalination 375 (2015) 100–107.
[19] M. Ghazy, A.A. Askalany, K. Harby, M.S. Ahmed, Adsorption isotherms and kinetics of HFC-404A onto bituminous based granular activated carbon for storage and cooling applications, Appl. Therm. Eng. 105 (2016) 639–645.
[20] F.N. Al-Mousawi, R. Al-Dadah, S. Mahmoud, Novel system for cooling and electricity: four different integrated adsorption-ORC configurations with two expanders, Energy Convers. Manag. 152 (2017) 72–87.
[21] E. Elsayed, P. Anderson, R. Al-Dadah, S. Mahmoud, A. Elsayed, MIL-101(Cr)/calcium chloride composites for enhanced adsorption cooling and water desalination, J. Solid State Chem. 277 (2019) 123–132.
[22] D.B. Boman, D.C. Hoysall, D.G. Pahinkar, M.J. Ponkala, S. Garimella, Screening of working pairs for adsorption heat pumps based on thermodynamic and transport characteristics, Appl. Therm. Eng. 123 (2017) 422–434.
[23] E. Elsayed, R. Al-Dadah, S. Mahmoud, A. Elsayed, P.A. Anderson, Aluminium fumarate and CPO-27(Ni) MOFs: characterization and thermodynamic analysis for adsorption heat pump applications, Appl. Therm. Eng. 99 (2016) 802–812.
[24] M.M. Saleh, R. Al-Dadah, S. Mahmoud, E. Elsayed, O. El-Samni, Wire fin heat exchanger using aluminium fumarate for adsorption heat pumps, Appl. Therm. Eng. 164 (2020).
[25] H.W.B. Teo, A. Chakraborty, Y. Kitagawa, S. Kayal, Experimental study of isotherms and kinetics for adsorption of water on aluminium fumarate, Int. J. Heat Mass Transf. 114 (2017) 621–627.
[26] E. Elsayed, R. Al-Dadah, S. Mahmoud, P. Anderson, A. Elsayed, Experimental testing of aluminium fumarate MOF for adsorption desalination, Desalination 475 (2020).
[27] E. Elsayed, R. Al-Dadah, S. Mahmoud, P. Anderson, A. Elsayed, Adsorption cooling system employing novel MIL-101(Cr)/CaCl2 composites: Numerical study, Int. J. Refrig. 107 (2019) 246–261.
[28] E. Elsayed, R. Al-Dadah, S. Mahmoud, P.A. Anderson, A. Elsayed, P.G. Youssef, CPO-27(Ni), aluminium fumarate and MIL-101(Cr) MOF materials for adsorption water desalination, Desalination 406 (2017) 25–36.
[29] B. Han, A. Chakraborty, Advanced cooling heat pump and desalination employing functional UiO-66 (Zr) metal-organic frameworks, Energy Convers. Manag. 213 (2020).
[30] K. Thu, A. Chakraborty, B.B. Saha, K.C. Ng, Thermo-physical properties of silica gel for adsorption desalination cycle, Appl. Therm. Eng. 50 (2) (2013) 1596–1602.
[31] T. Miyazaki, A. Akisawa, B.B. Saha, I.I. El-Sharkawy, A. Chakraborty, A new cycle time allocation for enhancing the performance of two-bed adsorption chillers, Int. J. Refrig. 32 (5) (2009) 846–853.
[32] K. Thu, B.B. Saha, A. Chakraborty, W.G. Chun, K.C. Ng, Study on an advanced adsorption desalination cycle with evaporator–condenser heat recovery circuit, Int. J. Heat Mass Transf. 54 (1–3) (2011) 43–51.
[33] K. Thu, Y.-D. Kim, A. Myat, A. Chakraborty, K.C. Ng, Performance investigation of advanced adsorption desalination cycle with condenser–evaporator heat recovery scheme, Desalin. Water Treat. 51 (1–3) (2012) 150–163.
[34] S. Mitra, P. Kumar, K. Srinivasan, P. Dutta, Performance evaluation of a two-stage silica gel + water adsorption based cooling-cum-desalination system, Int. J. Refrig. 58 (2015) 186–198.
[35] S.M. Ali, A. Chakraborty, Adsorption assisted double stage cooling and desalination employing silica gel + water and AQSOA-Z02 + water systems, Energy Convers. Manag. 117 (2016) 193–205.
[36] P.G. Youssef, S.M. Mahmoud, R.K. Al-Dadah, Numerical simulation of combined adsorption desalination and cooling cycles with integrated evaporator/condenser, Desalination 392 (2016) 14–24.
[37] J.W. Wu, M.J. Biggs, E.J. Hu, Dynamic model for the optimisation of adsorption-based desalination processes, Appl. Therm. Eng. 66 (1–2) (2014) 464–473.
[38] W. Yaïci, E. Entchev, Coupled unsteady computational fluid dynamics with heat and mass transfer analysis of a solar/heat-powered adsorption cooling system for use in buildings, Int. J. Heat Mass Transf. 144 (2019).
[39] W.D. Chen, K.J. Chua, Parameter analysis and energy optimization of a four-bed, two-evaporator adsorption system, Appl. Energy 265 (2020).
[40] R.H. Mohammed, O. Mesalhy, M.L. Elsayed, M.C. Su, L. Chow, Revisiting the adsorption equilibrium equations of silica-gel/water for adsorption cooling applications, Int. J. Refrig. 86 (2018) 40–47.
[41] F.N. Al-Mousawi, R. Al-Dadah, S. Mahmoud, Different bed configurations and time ratios: Performance analysis of low-grade heat driven adsorption system for cooling and electricity, Energy Convers. Manag. 148 (2017) 1028–1040.
[42] D. Cheng, E.A.J.F. Peters, J.A.M. Kuipers, Performance study of heat and mass transfer in an adsorption process by numerical simulation, Chem. Eng. Sci. 160 (2017) 335–345.
[43] İ. Solmuş, S. Andrew, D. Rees, C. Yamalı, D. Baker, A two-energy equation model for dynamic heat and mass transfer in an adsorbent bed using silica gel/water pair, Int. J. Heat Mass Transf. 55 (19–20) (2012) 5275–5288.
[44] M.A. Aziz, I.A.M. Gad, E.S.F.A. Mohammed, R.H. Mohammed, Experimental and numerical study of influence of air ceiling diffusers on room air flow characteristics, Energy Build. 55 (2012) 738–746.
[45] R.H. Mohammed, A simplified method for modeling of round and square ceiling diffusers, Energy and Buildings 64 (2013) 473–482.
[46] R.H. Mohammed, O. Mesalhy, M.L. Elsayed, L.C. Chow, Scaling analysis of heat and mass transfer processes in an adsorption packed bed, Int. J. Therm. Sci. 133 (2018) 82–89.
[47] H.T. El-Dessouky, H.M. Ettouney, Fundamentals of Salt Water Desalination, Elsevier Science B.V., 2020.
[48] I.S. Glaznev, Y.I. Aristov, The effect of cycle boundary conditions and adsorbent grain size on the water sorption dynamics in adsorption chillers, Int. J. Heat Mass Transf. 53 (9–10) (2010) 1893–1898.
[49] H. Ramy, Osama Mohammed, Mohamed Mesalhy, et al., Assessment of numerical models in the evaluation of adsorption cooling system performance - ScienceDirect, Int. J. Refrig. 99 (2019) 166–175.
[50] M. Mohammadzadeh Kowsari, H. Niazmand, M.M. Tokarev, Bed configuration effects on the finned flat-tube adsorption heat exchanger performance: Numerical modeling and experimental validation, Appl. Energy 213 (2018) 540–554.